PHYSICAL REVIEW C VOLUME 25, NUMBER 1 JANUARY 1982

Neutron capture in the giant resonance region of ^{15}N

S. A. Wender, H. R. Weller, and N. R. Roberson
Duke University and Triangle Universities Nuclear Laboratory, Duke Station, Durham, North Carolina, 27706

D. R. Tilley
North Carolina State University, and Triangle Universities Nuclear Laboratory, Durham, North Carolina, 27706

R. G. Seyler
The Ohio State University, Department of Physics, Columbus, Ohio 43210
(Received 8 June 1981)

The $^{14}N(n,\gamma_0)^{15}N$ reaction has been studied over a neutron energy range of 5.6 MeV to 13 MeV. Data include a 90° excitation function measured in 200 keV steps, and seven angular distributions. The angular distribution data show good agreement with the results of a phenomenological direct semidirect model calculation. No non-$E1$ radiation is required to account for these data. The cross section as a function of energy is similar to the $^{14}N(p,\gamma_0)^{15}O$ reaction and different from the $^{14}C(p,\gamma_0)^{15}N$ reaction. These differences can be understood in terms of the different isospin states allowed in each reaction.

[NUCLEAR REACTIONS $^{14}N(n,\gamma_0)^{15}N$, measured $\sigma(E,\theta)$ from $E_n=5.6-13.0$ MeV, DSD model calculations, results compared to $^{14}C(p,\gamma_0)^{15}N$ and $^{14}N(p,\gamma_0)^{15}O$.]

INTRODUCTION

The giant dipole resonance (GDR) of ^{15}N has been the topic of interest in a significant number of capture reaction studies. Several groups have reported measurements of the $^{14}C(p,\gamma_0)^{15}N$ reaction using polarized[1,2] and unpolarized[3] beams. Del Bianco *et al.*[4] have measured the $^{11}B(\alpha,\gamma_0)^{15}N$ reaction, and Schaeffer *et al.*[5] have studied the $^{12}C(t,\gamma_0)^{15}N$ reaction. Weller and Blue,[6] Del Bianco *et al.*[7] and Skopik *et al.*[8] have investigated the $^{13}C(d,\gamma_0)^{15}N$ reaction including an angular distribution measurement with a vector polarized deuteron beam.[8] The results of these experiments have indicated that the reaction mechanism is rather complex, since the structures in the cross section seen in the various capture channels do not appear to be correlated in any obvious way. Since the composite particle channels are competitive with single nucleon ground state channels, it would appear that a 2h-1p shell model basis is not an adequate description of the GDR in this case. However, it should be noted that the capture reaction does not readily populate the $(p_{3/2}^{-1}p_{1/2}^{-1})\otimes d_{5/2}$ configuration which is presumed to be a large component of the GDR.

Although there have been a large number of studies of the GDR region of ^{15}N, there has been one conspicuous omission: the neutron channel. In the present paper we shall present the results of our investigation of the $^{14}N(n,\gamma_0)^{15}N$ reaction. In addition to completing the major capture experiments into ^{15}N, the $^{14}N(n,\gamma_0)^{15}N$ reaction study should be of interest with regard to the isospin structure of the GDR region of ^{15}N. In the absence of isospin mixing, a comparison of the $^{14}C(p,\gamma_0)^{15}N$ reaction, which should populate states with $T=\frac{1}{2}$ and $\frac{3}{2}$, with the $^{14}N(n,\gamma_0)^{15}N$ reaction, which should only populate $T=\frac{1}{2}$ states, should allow at least a tentative identification of $T=\frac{3}{2}$ strength in ^{15}N. Previous efforts on this problem[3] have used the $^{14}N(p,\gamma_0)^{15}O$ (Ref. 9) data which should display the $T=\frac{1}{2}$ strength in the mirror nucleus ^{15}O. As we shall see below, this comparison may be complicated if there is any energy shift between the structures in the GDR's of these mirror nuclei.

A neutron capture study also promises to shed

light on the nature of the non-$E1$ radiation present in the experiment. Recent polarized proton capture studies on 1p-shell nuclei have indicated that the observed non-$E1$ effects can be accounted for by the presence of direct $E2$ capture radiation. Since the direct $E2$ amplitude is scaled by the kinematic effective charge, which is smaller for neutrons as compared to protons, the direct $E2$ effects should essentially vanish in the neutron capture experiment.[10] The fact that the neutron capture process should not contain any significant direct $E2$ capture should increase its sensitivity to the presence of collective $E2$ capture amplitudes.

EXPERIMENTAL

A diagram of the apparatus is shown in Fig. 1. The neutron beam was produced using the $^2H(d,n)^3He$ reaction. The deuterium gas cell was a 3.0 cm long cell with a 4 mg/cm^2 thick molybdenum entrance window, and was pressurized to two atmospheres. The energy spread in the neutron beam from this cell varied from approximately 250 keV at $E_n = 6.0$ MeV to 100 keV at $E_n = 13.0$ MeV. The absolute energy of the neutron beam was calibrated to within 50 keV using a resonance in the $^{12}C(n,n)^{12}C$ cross section at 6.30 MeV.[11]

The target was prepared by compressing Be_3N_2 powder into a thin walled plexiglas cylinder 3.8 cm high and 3.8 cm in diameter. The resulting target had a measured density of 1.55 g/cm^3 and contained 34.2 g of nitrogen. The center of the target was located 7.8 cm from the end of the deuterium gas cell.

The γ rays were detected in a spectrometer consisting of a 25.4 cm by 25.4 cm NaI crystal and a plastic anticoincidence shield. This system has been previously described in detail.[1] As shown in Fig. 1, the detector was shielded from the direct neutron flux emanating from the gas cell by means of a tungsten "shadow bar." In order to improve the signal to noise ratio the beam was chopped and bunched at a rate of 2 MHz into pulses approximately 2 nsec wide. A typical time of flight spectrum is shown in Fig. 2. By setting a digital window with the proper time-of-flight criterion, we were able to distinguish prompt γ rays from the subsequent burst of neutrons.

Since the Q value of the reaction is large ($+10.836$ MeV), and the γ_0 transition is well separated from the first excited state, we operated the spectrometer with a high threshold on the shield energy discriminator. This resulted in a larger γ-ray efficiency for the detector but with some decrease in energy resolution. In this mode the detector had an efficiency of 27% and an energy resolution of approximately 5%, for γ-ray energies around 20 MeV.

The value of the detector efficiency is based on the measured thick target yield of the $^{12}C(p,\gamma)$ reaction[12] at 15.07 MeV. The energy dependence

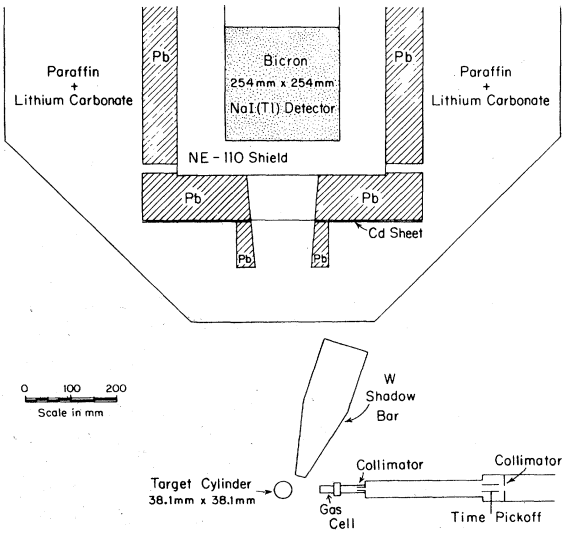

FIG. 1. Schematic diagram of the detector system, the gas cell, and the target geometry.

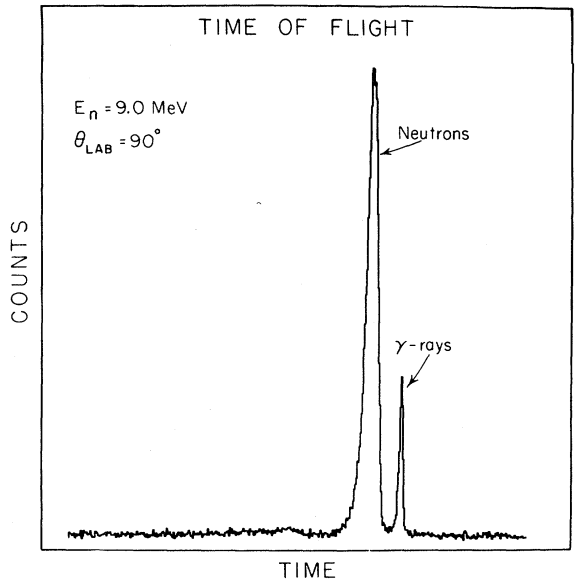

FIG. 2. Typical time of flight spectrum showing separation of neutron and γ-ray events in the detector.

of the efficiency was taken to be a constant[13] over the energy range covered in this experiment.

RESULTS

The 90° excitation function for the $^{14}N(n,\gamma_0)^{15}N$ reaction was measured in 200 keV steps for neutron energies between 5.6 and 13 MeV. This energy range corresponds to 16.0 to 24.0 MeV excitation in ^{15}N. A typical spectrum is shown in Fig. 3. The number of counts in the peaks were obtained by fitting the data to a standard line shape, and the yields were corrected for dead time and accidental count rate effects. The average beam current on target ranged from 100 to 400 nA. Each data point contained approximately 200 counts and required appoximately 2 h to acquire.

In order to calculate an absolute value for the capture cross section, several corrections must be applied to the data. These corrections are basically due to the finite extent of the neutron source and the finite size of the sample and the detector. The neutron flux, which has a forward-peaked angular distribution, must be averaged over the volumes of the gas cell and sample. The cross section and angular distributions for the $^2H(d,n)^3He$ reaction were taken from Drosg.[14] Corrections must also be made for the attenuation of the neutron flux and the γ rays in the sample. In addition, corrections must be made for events which arise from the multiple scattering of neutrons. These averages were performed using a Monte Carlo simulation computer program. Since the sample contained both beryllium and nitrogen, we corrected for multiple scattering using the Monte Carlo simulation program for two limiting cases: a pure beryllium sample and a pure nitrogen sample. The multiple scattering corrections differed in these two cases by less than 3%, and we corrected the data with their average values.

The 90° excitation function, corrected as described above, is plotted in Fig. 4 as a function of incident neutron energy. The errors shown in Fig. 4 represent only the statistical errors. We estimate an overall uncertainty of 20% in the absolute cross section.

Angular distributions were obtained at incident neutron energies of 7.0, 7.8, 9.2, 9.8, 10.4, 12.0, and 13.0 MeV. Corrections were made, as described above, and the corrected angular distributions were fit to an expansion in Legendre polynomials:

$$\frac{d\sigma(\theta)}{d\Omega} = A_0 \left[1 + \sum_{k=1}^{N} a_k P_k(\cos\theta) \right] . \quad (1)$$

Typical data and fits are shown in Fig. 5. It was

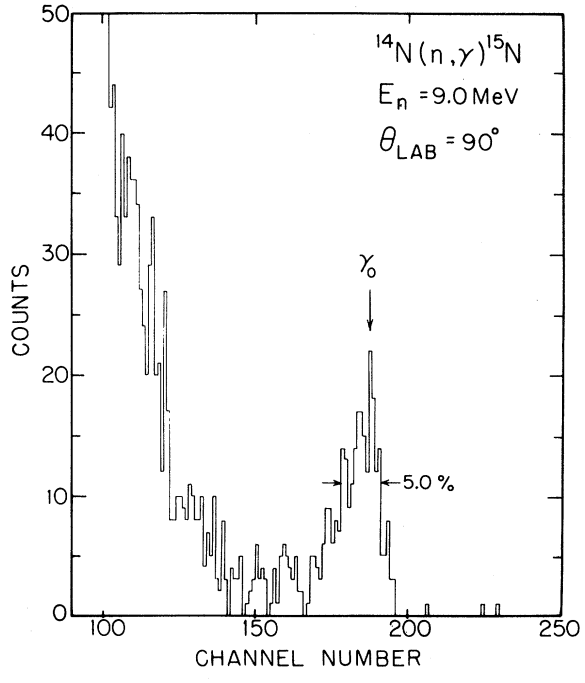

FIG. 3. Energy spectrum observed at $E_n = 9.0$ MeV for the $^{14}N(n,\gamma_0)^{15}N$ reaction at 90 deg. This spectrum was obtained with decreased energy resolution in order to increase the detector efficiency.

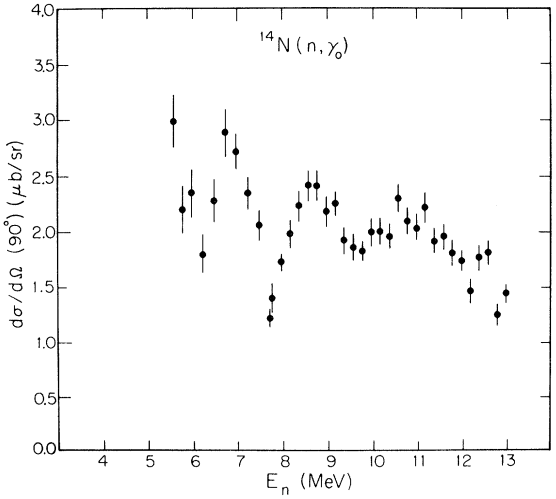

FIG. 4. Cross section at 90 deg for the $^{14}N(n,\gamma_0)^{15}N$ reaction as a function of incident neutron energy. The error bars shown represent only statistical errors.

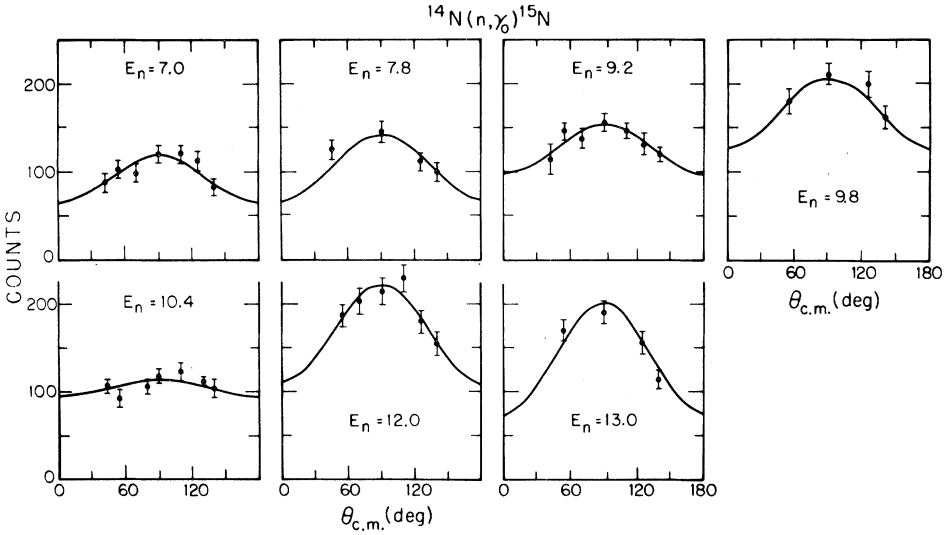

FIG. 5. γ-ray angular distributions for the $^{14}N(n,\gamma_0)^{15}N$ reaction. Curves are the results of Legendre polynomial fits to the data. Error bars represent statistical errors.

found that satisfactory fits (i.e., $\chi^2 \sim 1$) were obtained when only terms through order $k=2$ were included. The results of the fit for a_1 and a_2 plotted versus neutron energy in ^{15}N, are shown in Fig. 6.

DISCUSSION

The direct semidirect (DSD) model has had considerable success in describing the general features of proton and neutron capture reactions.[15–17] In this model, for the case of electric transitions, the radial transition matrix elements, (T_{lj}^L) are of the form:

$$T_{lj}^L \propto \left\langle u_{l'j'}(r) \left| q_{\text{eff}} r^L + \frac{h(r)}{E - E_d + \frac{i\Gamma_d}{2}} \right| \chi_{lj}(r) \right\rangle , \tag{2}$$

where $u_{l'j'}(r)$ is the bound state radial wave function, $\chi_{lj}(r)$ is the radial part of the neutron partial wave in the incident channel, and r^L is the single particle electromagnetic operator of multipolarity L in the long wavelength limit. E_d and Γ_d are the position and width of the resonance. Note that the kinematic effective charge, q_{eff}, scales the direct amplitude. If the form factor, $h(r)$, is set to zero, the matrix element describes direct capture. If we assume that the resonance parameters are the same for all l and j and choose $h(r) \propto r^L$ as suggested by Brown,[18] then the relative amplitudes of the DSD model are the same as for the pure direct model.

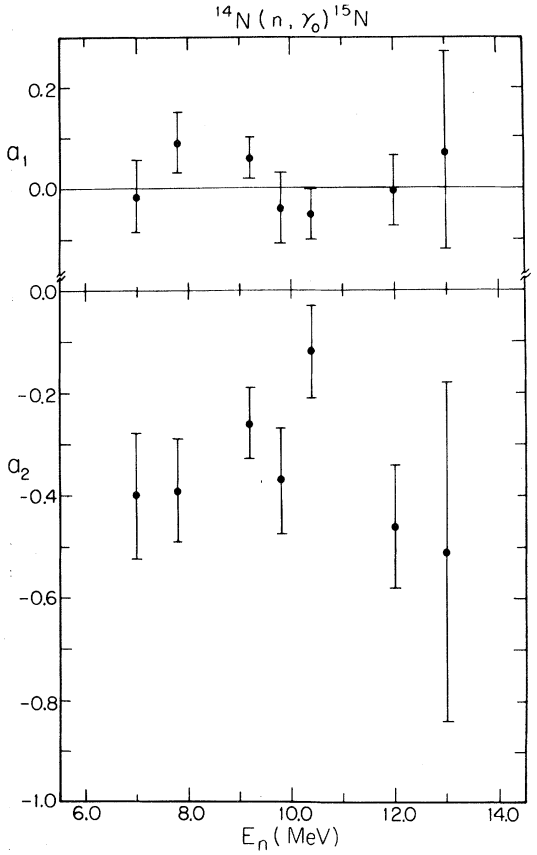

FIG. 6. Coefficients resulting from the Legendre polynomial fits to the angular distributions plotted as a function of γ-ray energy. The error bars represent the statistical errors associated with these coefficients.

Other expressions for $h(r)$ have been suggested.[19]

In the case of $^{14}N+n$, with a target spin $j_a=1$, it is possible to have 5 $E1$ and 6 $E2$ matrix elements. Since these matrix elements are complex, we have 11 amplitudes and 10 relative phases for a total of 21 unknowns. If we assume that the spin of the target is ineffective in determining the value of these matrix elements, then we can write the matrix element for the spin j_a target in terms of a spin-zero target matrix element:

$$\langle Lj_cj_b \,||\, T \,||\, (lx)jj_aj_b \rangle = \sum_{j'} \langle Lj'j \,||\, T \,||\, (lx)j0j \rangle \sqrt{(2j+1)}\sqrt{(2j_c+1)}\, W(j_aj'j_bL;j_cj) \,, \tag{3}$$

where we couple the orbital angular momentum l, and the spin x of the projectile to a total angular momentum j. The angular momentum of the γ-emitting state is j_b, j' is the angular momentum of the single particle in the final state, and j_c is the spin of the final nucleus obtained by coupling j' and j_a.

It can be shown that this relationship implies that the equations to be used to express the non-zero spin target angular distribution coefficients in terms of the spin-zero target matrix elements are essentially the target spin-zero equations where the final state has a total angular momentum j'. If we use the $j-j$ coupling scheme and label the contributing matrix elements by the orbital angular momentum and total angular momentum (l,j) of the projectile and the multipolarity of the outgoing radiation (L), then we can define a matrix element having amplitude $l_j(L)$ and phase (l). The equations for the a_1 and a_2 coefficients in terms of the amplitudes and phases of the $E1$ and $E2$ target spin-zero matrix elements are[17]

$$\begin{aligned}
1 &= s_{1/2}(E1)^2+2d_{3/2}(E1)^2+2p_{3/2}(E2)^2 \\
&\quad +3f_{5/2}(E2)^2 \ \text{(normalization)} \,, \\
a_1 &= 3.464 s_{1/2}(E1)p_{3/2}(E2)\cos(s-p) \\
&\quad +0.6928 d_{3/2}(E1)p_{3/2}(E2)\cos(d-p) \\
&\quad +6.235 d_{3/2}(E1)f_{5/2}(E2)\cos(d-f) \,, \\
a_2 &= -2s_{1/2}(E1)d_{3/2}(E1)\cos(s-d) \\
&\quad -d_{3/2}(E1)^2+p_{3/2}(E2)^2 \\
&\quad +0.8571 p_{3/2}(E2)f_{5/2}(E2)\cos(p-f) \\
&\quad +1.714 f_{5/2}(E2)^2 \,.
\end{aligned} \tag{4}$$

These equations enable us to evaluate the angular distribution coefficients from the calculated target spin-zero matrix elements for comparison with the data. The cross section for the case of a target with spin j_a is related to the spin-zero target cross section by:

$$\sigma_t(\text{target spin } j_a) = \frac{2j_c+1}{(2j_a+1)(2j'+1)} \sigma_t(\text{target spin } 0, \text{residual } j') \,. \tag{5}$$

We have calculated the relative amplitudes and phases for the $^{14}N(n,\gamma_0)$ reaction using a phenomenological DSD model in the following way. We first calculated the results for pure direct $E1$ capture of a neutron into a $p_{1/2}$ orbital assuming a target spin of zero. This calculation used the optical model parameters compiled by Perey and Perey[20] to construct the continuum wave function, and a Woods-Saxon potential adjusted to give the experimental binding energy of the $p_{1/2}$ single particle state in the ground state of ^{14}N to construct the bound state wave function. The spectroscopic factor ($S=1.45$) was taken from the recent measurements of Kretschmer *et al.*[21] Since the yield curve does not show a well defined resonance shape, we constructed an $E1$ semidirect term by normalizing the calculated direct $E1$ cross section to the data at each excitation energy. In this way we can calculate the relative magnitudes and phases of the spin-zero matrix elements assuming a form factor proportional to r without having to specify resonance parameters. The $E2$ cross section was calculated as pure direct.

The equations given above were used to obtain the a_1 and a_2 angular distribution coefficients from the calculated target spin-zero amplitudes and phases. We also calculated the angular distribution coefficients for the $^{14}C(p,\gamma_0)^{15}N$ and the $^{14}N(p,\gamma_0)^{15}O$ reactions in a similar manner. Since the set of equations for the angular distribution coefficients for the $^{14}N+p$ reaction can be expressed in terms of the spin-zero target matrix ele-

ments, all three reactions have the same equations. Figure 7 shows the results of these calculations along with the published data[1–3,9] on these reactions.

As seen in Fig. 7, the general features of the angular distribution coefficients are reasonably well predicted by this phenomenological DSD model for each of these three reactions. The small a_1

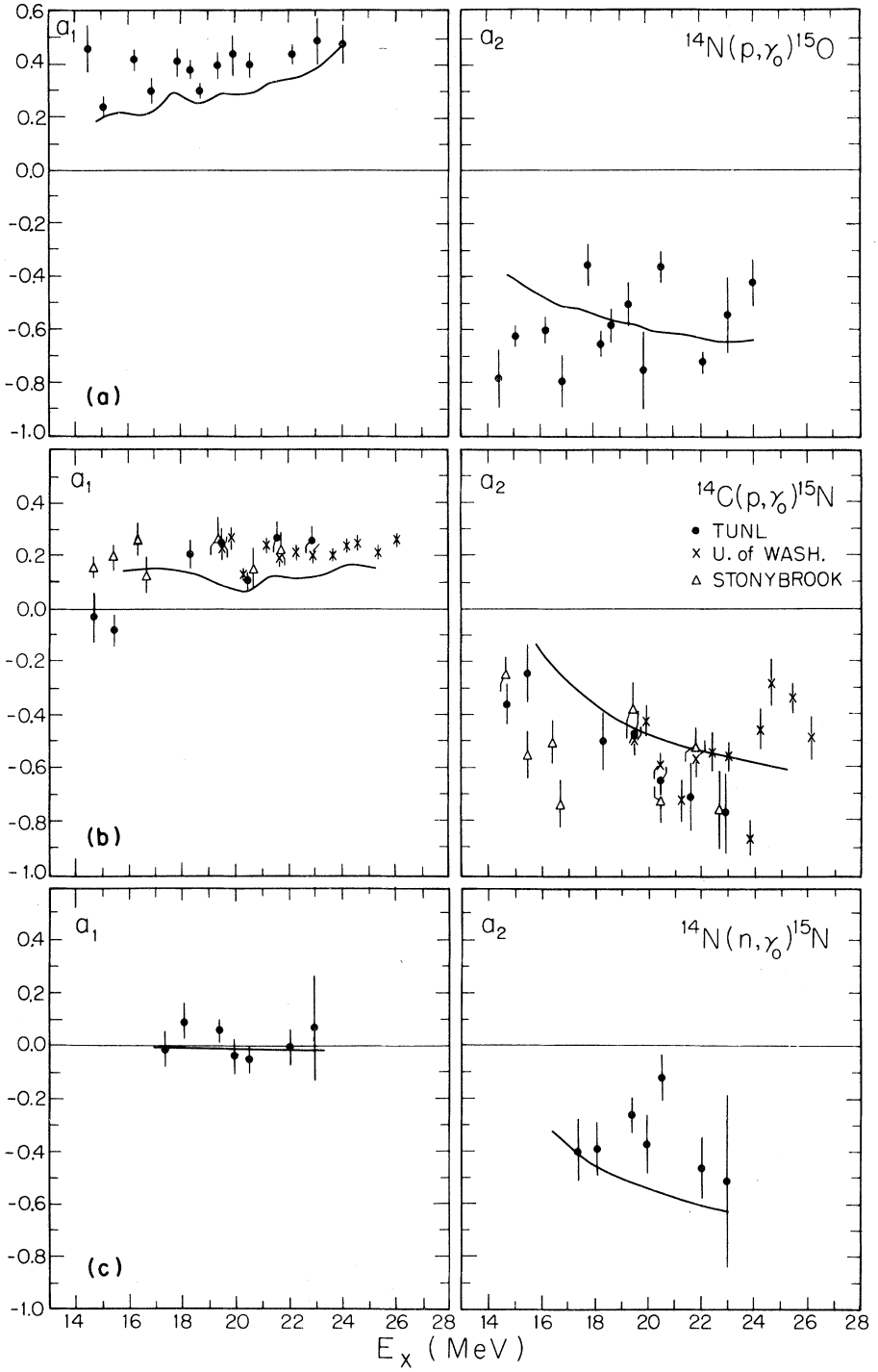

FIG. 7. Angular distribution coefficients for (a) $^{14}N(p,\gamma_0)$ (Ref. 9), (b) $^{14}C(p,\gamma_0)$, and (c) $^{14}N(n,\gamma_0)$ (present work) reactions. Also shown are results of phenomenological DSD calculations as described in the text. TUNL Ref. 1; University of Washington, Ref. 2; Stony Brook, Ref. 3.

coefficient calculated in the case of neutron capture comes from the small neutron effective charge for $E2$ radiation, while the larger a_1 coefficients predicted for the proton capture reactions are the result of the greater proton $E2$ effective charge. This behavior is supported nicely by the data. This projectile dependence of the a_1 coefficients suggests that the large a_1 coefficients observed in the proton capture are due primarily to direct $E2$ capture amplitudes. The fact that we measured an essentially zero a_1 coefficient is consistent with little or no non-$E1$ radiation in this energy range for the ground state neutron channel, at least within the accuracy of our experiment. A more definite statement on the $E2$ strength in this reaction must await more accurate measurements of angular distributions of cross sections as well as measurements with polarized beams.

The general similarity of the calculated a_2 coefficients in these three $A=15$ reactions is due primarily to the dominance of $E1$ radiation and the similarity of the potentials which determine the relative amplitudes and phases of the contributing matrix elements. The fluctuations in the a_2 coefficients are an indication of more complicated interactions than included in the simple DSD model used here.

It is also interesting to compare the cross sections for the three $A=15$ reactions. The $^{15}\mathrm{N}(\gamma,n_0)$ and the $^{15}\mathrm{O}(\gamma,p_0)$ reactions should proceed only through $T=\frac{1}{2}$ states, while the $^{15}\mathrm{N}(\gamma,p_0)$ reaction allows both $T=\frac{1}{2}$ and $T=\frac{3}{2}$ states. Figure 8 shows the excitation function for the $^{15}\mathrm{O}(\gamma,p_0)$,[9] $^{15}\mathrm{N}(\gamma,p_0)$,[1] and $^{15}\mathrm{N}(\gamma,n_0)$ reactions. These results were obtained from the capture data using the principle of detailed balance. A comparison of the two $^{15}\mathrm{N}$ reactions shows that the yield in the neutron channel is smaller and has less structure. This suggests that the large peaks at 19.5 and 20.5 MeV and the smaller peak at 21.6 MeV observed in the proton channel are likely to be primarily $T=\frac{3}{2}$ states.

On the other hand, the $^{14}\mathrm{N}+p$ and the $^{14}\mathrm{N}+n$ cross sections look remarkably similar. The yields are approximately equal in magnitude over the measured energy range. The two prominent dips at $E_x=16.7$ and 18.1 MeV observed in the $^{14}\mathrm{N}+n$ reaction are also seen in the $^{14}\mathrm{N}+p$ reaction at $E_x=16.3$ and 17.7 MeV. If these two structures are correlated, the reason for their 400 ± 100 keV difference in energy is not obvious. On the basis of Coulomb energies, if we assume a ground state radius of 2.65 fm,[22] and a ground state Coulomb

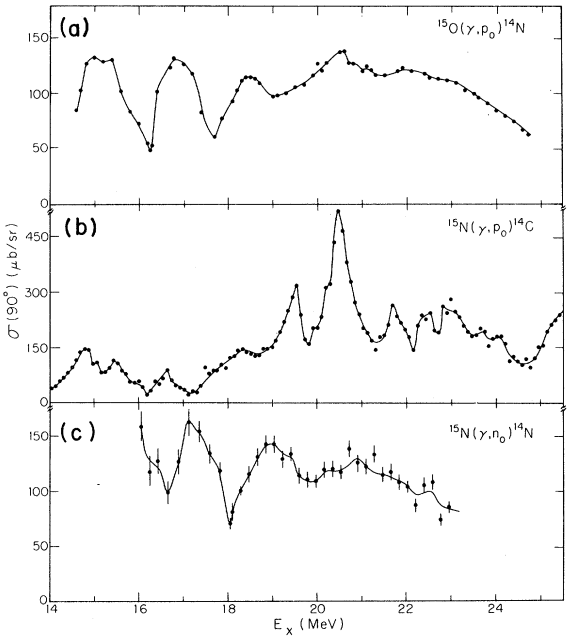

FIG. 8. Cross section at 90 deg as function of excitation energy for (a) $^{15}\mathrm{O}(\gamma,p_0)$, (b) $^{15}\mathrm{N}(\gamma,p_0)$, and (c) $^{15}\mathrm{N}(\gamma,n_0)$ reactions.

energy difference of 3.54 MeV,[23] a 400 ± 100 keV shift would correspond to a change in radius relative to the ground state of 0.3 ± 0.08 fm.

In view of this energy shift, it would appear to be incorrect to correlate structures in the $^{14}\mathrm{C}(p,\gamma)^{15}\mathrm{N}$ and the $^{14}\mathrm{N}(p,\gamma)^{15}\mathrm{O}$ which occur at the same excitation energy. Thus some of the conclusions of Ref. 3 regarding the isospin identifications appear to be suspect.

If the cross section obtained in the present work is detailed balanced and integrated over energy and angle, it is found that the neutron channel exhausts about 4% of the classical dipole sum. About 6% of this sum has been previously observed in the (γ,p_0) channel, while the (γ,α_0) and the (γ,d_0) channels indicate approximately 2% and 1%, respectively. These values support the contention that the composite particle channels are not negligible with respect to the single nucleon ground state channels in the GDR of $^{15}\mathrm{N}$.

CONCLUSION

With this investigation of the $^{14}\mathrm{N}(n,\gamma_0)$ reaction we have obtained data for a previously unstudied capture channel into $^{15}\mathrm{N}$. The gross behavior of

the cross section in the giant resonance region is similar to that of the $^{14}N+p$ reaction which also only populates $T=\frac{1}{2}$ isospin states, and is different from the $^{14}C(p,\gamma_0)$ reaction in which both $T=\frac{1}{2}$ and $\frac{3}{2}$ states can be populated. The behavior of the angular distribution coefficients is in general agreement with a phenomenological DSD model calculation, and within the precision of this experiment does not indicate the presence of any $E2$ radiation in the neutron channel over the energy region studied. On the other hand, the differences between the present DSD calculations and the experiment emphasize the fact that other processes such as compound nucleus formation may also be involved here or, in fact, the form of Eq. (2) may need to be modified. Finally, a comparison of the structures in the giant resonance region of ^{15}N and ^{15}O indicates that there is an energy difference of approximately 400 keV between them.

[1]H. R. Weller, R. A. Blue, N. R. Roberson, D. G. Rickel, S. Maripuu, C. P. Cameron, R. D. Ledford, and D. R. Tilley, Phys. Rev. C 13, 922 (1976).
[2]K. A. Snover, J. E. Bussoletti, K. Ebisawa, T. A. Trainor, and A. B. McDonald, Phys. Rev. Lett. 37, 273 (1976).
[3]M. H. Harakeh, P. Paul, H. M. Kuan, and E. K. Warburton, Phys. Rev. C 12, 1410 (1975).
[4]W. Del Bianco, S. Kundu, and J. Kim, Can. J. Phys. 55, 302 (1977).
[5]M. Schaeffer, A. Degre, M. Suffert, G. Bonneaud, and I. Linck, Nucl. Phys. A275, 1 (1977).
[6]H. R. Weller and R. A. Blue, Nucl. Phys. A211, 221 (1973).
[7]W. Del Bianco, S. Kundu, and J. Kim, Nucl. Phys. A270, 45 (1976).
[8]D. M. Skopik, J. J. Murphy II, H. R. Weller, R. A. Blue, N. R. Roberson, S. A. Wender, and D. R. Tilley. Phys. Rev. C 20, 409 (1979).
[9]H. M. Kuan, M. Hansinoff, W. J. O'Connell, and S. S. Hanna, Nucl. Phys. A151, 129 (1970).
[10]E. D. Arthur, D. M. Drake, and I. Halpern, Phys. Rev. Lett. 35, 914 (1975).
[11]S. Cierjack *et al.*, Nucl. Instrum. Methods 169, 185 (1980).
[12]R. E. Marrs, E. G. Adelberger, K. A. Snover, and M. D. Cooper, Phys. Rev. Lett. 35, 202 (1975).
[13]H. R. Weller, N. R. Roberson, IEEE NS-28, 1268 (1981).
[14]M. Drosg, Nucl. Sci. Eng. 67, 190 (1978).
[15]I. Bergqvist and M. Potokar in *Neutron Capture Gamma-Ray Spectroscopy,* edited by Robert Chrien and Walter R. Kane (Plenum, New York, 1979), p. 299.
[16]K. A. Snover, in *Neutron Capture Gamma-Ray Spectroscopy,* edited by Robert Chrien and Walter R. Kane (Plenum, New York, 1979), p. 319.
[17]H. R. Weller and N. R. Roberson, Rev. Mod. Phys. 52, 699 (1980).
[18]G. E. Brown, Nucl. Phys. 57, 339 (1964).
[19]M. Potokar, A. Likar, M. Budnar, and F. Cvelbar, Nucl. Phys. A277, 29 (1977).
[20]C. M. Perey and F. G. Perey, Nucl. Data Tables 13, 293 (1974).
[21]W. Kretschmer *et al.*, Nucl. Phys. A333, 13 (1980).
[22]C. W. de Jager, H. de Vries, and C. de Vries, At. Data Nucl. Data Tables 14, 479 (1974).
[23]W. J. Courtney and J. D. Fox, At. Data Nucl. Data Tables 15, 141 (1975).